IEEE Access
Multidisciplinary | Rapid Review | Open Access Journal

Received August 30, 2021, accepted September 26, 2021, date of publication September 29, 2021, date of current version October 7, 2021.

Digital Object Identifier 10.1109/ACCESS.2021.3116761

Dynamic Performance Enhancement Method Based on Improved Model Reference Adaptive System for SPMSM Sensorless Drives

YIRONG TANG, (Student Member, IEEE), WEI XU, (Senior Member, IEEE), YI LIU, (Senior Member, IEEE), AND DINGHAO DONG, (Graduate Student Member, IEEE)
State Key Laboratory of Advanced Electromagnetic Engineering and Technology, Huazhong University of Science and Technology, Wuhan 430074, China

Corresponding author: Wei Xu (weixu@hust.edu.cn)

This work was supported in part by the National Natural Science Foundation of China under Grant 51877093, in part by the National Key Research and Development Program of China under Grant YS2018YFGH000299, and in part by the Key Technical Innovation Program of Hubei Province under Grant 2019AAA026.

ABSTRACT Conventional sensorless drives usually suffer from an unsatisfactory dynamic response to the varying speed reference or load disturbance due to the design only for the speed estimator. In this paper, an improved adaptive law based model reference adaptive system (IAL-MRAS) algorithm is proposed to enhance the dynamic performance of a surface-mounted permanent magnet synchronous motor (SPMSM) sensorless drives, in which both a speed/position estimator and composite speed controller are designed by a systematic way. This improved adaptive law (IAL) incorporates both the mechanical and electromagnetic model to account for the mechanical factors on the speed variation, which can estimate the rotor position and load torque simultaneously. To further strengthen the disturbance rejection ability, a composite speed controller is designed based on the feedforward compensation scheme and IAL-MRAS. Meanwhile, a hybrid control strategy combining IAL-MRAS and *I-f* starting method is adopted to realize sensorless control in the full speed range. Comprehensive numerical simulation and experimental results have fully demonstrated that the proposed sensorless control strategy can achieve smaller settling time, stronger disturbance rejection ability, and less parameter tuning workload than those of the conventional methods.

INDEX TERMS Feedforward compensation, improved adaptive law (IAL), model reference adaptive system (MRAS), sensorless control, surface-mounted permanent magnet synchronous motor (SPMSM).

I. INTRODUCTION

Permanent magnet synchronous motors (PMSMs) have been widely used in electrical vehicle, rail transit and other fields owing to their advantages of high efficiency, high reliability, *etc*. In general, the mechanical sensor such as optical encoder or resolver can provide the necessary rotor position for a PMSM control system, which leads to higher cost and lower reliability. In applications that are sensitive to cost or need to provide redundant control solutions, the sensorless control strategy can be a better choice [1], [2].

Generally, the sensorless control methods for PMSM can be divided into two categories, i.e. high-frequency injection (HFI) and back electromotive force (EMF) model [3]. The first method takes advantage of the anisotropic properties of the machines which is suitable for zero-low speed range, and the second method is generally used for medium-high speed range when the back EMF or speed-dependent voltages are big enough for extracting. Currently, the sensorless control algorithms based on back EMF model have been implemented by various methods, including sliding mode observer (SMO) [4]–[6], extended Kalman filter (EKF) [7], state observer method [8], [9], and model reference adaptive system (MRAS) [10]–[15], *etc*. Among them, the MRAS-based methods have drawn attention due to their simplicity. In contrast to the HFI, the model based methods are generally not suitable at low speed. To solve this problem, a combination of the two methods is desirably needed. In [16], a hybrid control strategy integrating with an improved flux linkage observer and the *I-f* starting method is proposed. Meanwhile, Refs. [13] and [15] combine MRAS with another method such as HFI to realize an accurate detection of rotor position in the full

The associate editor coordinating the review of this manuscript and approving it for publication was Jinquan Xu.

speed range. So far, great contributions have been made to the PMSM sensorless drives, and the main attentions have been paid on the solutions for achieving higher accuracy and wider operation range.

However, most sensorless control methods are based on the electromagnetic model of PMSM only, and cannot account for the impacts of mechanical factors on the performance. It is worth noting that using mechanical model is an effective way to consider mechanical factors and get more information about the drive system. Thus, some sensorless control methods incorporating both electromagnetic and mechanical model are proposed to improve the system performance in [17]–[19]. In [17], an electromagnetic torque-based MRAS is proposed based on the mechanical model that can work in wide speed range. The mechanical model is used to build an extended sliding mode mechanical parameter observer in [18], which can estimate the load torque and inertia. In [19], a full state estimator with speed and rotor position as state variables is constructed while the mechanical model is used to estimate external disturbance. These studies have demonstrated the effectiveness of mechanical model in load disturbance estimation and performance enhancement.

The dynamic performance for PMSM sensorless drives mainly depends on two aspects, i.e. the speed/position estimation algorithms as aforementioned, and the speed controller. The design of speed controller is another crucial problem for the sensorless drives, which have not been paid enough attentions till now. For the simple control structure, the PI controller is still widely used in speed regulation, while it usually suffers from the contradictions between the speed tracking and load disturbance rejection properties [20]. Hence, the tuning of PI gains is a matter of trade-off. Due to this, many advanced speed control strategies have been focused to improve the drive performance of the PMSM [21]–[25]. In [23], a new continuous fast terminal sliding mode control (SMC) is proposed for the speed regulation, which introduces an extended state observer (ESO) to estimate the system disturbances for the feedforward compensation. However, the mathematical complexity of reaching law and the inevitable chattering phenomenon in SMC are still uphill tasks. Then, an active disturbance rejection control with ESO is proposed in [24], which can provide strong robustness and superior transient. Meanwhile, the load torque sliding mode observer is used to realize the feedforward in [25], while the influence of load torque can be suppressed. However, compared with the speed sensed drives, it should be noted that an extra dynamic between the estimated and actual speed/position exists in the sensorless drives. Hence, the advanced control methods used in the sensed drives cannot be directly adopted for sensorless drives. If this extra dynamic is ignored in the implementation of these advanced methods for the sensorless drives, not only the expected performance improvements cannot be achieved, but also an unwanted stability problem might be induced [26]. Thus, further investigation on the sensorless control methods is required and the estimator and controller should be designed systematically.

From the aforementioned, this paper aims to improve the dynamic performance for SPMSM sensorless drives with an improved adaptive law based MRAS (IAL-MRAS) by designing the speed/position estimator and the speed controller simultaneously. In this method, the speed/position estimator is developed by the IAL-MRAS, which is based on both the mechanical and electromagnetic model. Compared with the conventional MRAS method, the proposed IAL-MRAS can estimate two parameters (speed and load torque) with single PI gains. Moreover, with the load torque estimated by IAL-MRAS, the feedforward compensation is considered to put forward a speed controller, which has strong disturbance rejection ability to load variations and fast dynamic response. Meanwhile, *I-f* control strategy is applied to realize startup and low speed operation, so that a full speed range sensorless control can be achieved. Simulation and experimental results on an SPMSM drive system are presented to validate the effectiveness and feasibility of the proposed method.

This paper is organized as follows. In Section II, the improved adaptive law in IAL-MRAS is analyzed and designed, then one speed controller based on IAL-MRAS and *I-f* startup strategy is presented in Section III. Section IV illustrates comprehensive simulation and experimental results during different working states. Finally, conclusions are drawn in Section V.

II. IMPROVED ADAPTIVE LAW BASED ON MRAS

A. THE PMSM DRIVE SYSTEM MODELLING

Ignoring some factors such as iron loss, crossing-coupling magnetic saturation and magnet eddy current loss, *etc*., the general mathematical model of PMSM in the d-q reference frame can be illustrated as

$$u_d = R_s i_d + L_d \frac{di_d}{dt} - \omega_e L_q i_q \tag{1}$$

$$u_q = R_s i_q + L_q \frac{di_q}{dt} + \omega_e L_d i_d + \omega_e \psi_f \tag{2}$$

$$T_e = \frac{3}{2} n_p [\psi_f i_q + (L_d - L_q) i_d i_q] \tag{3}$$

$$T_e - T_L = J \frac{d\omega_r}{dt} \tag{4}$$

where u_d and u_q are the d- and q-axis stator voltages, i_d and i_q the d- and q-axis stator currents, R_s is the stator resistance, L_d and L_q are the d- and q-axis inductances, ψ_f is the rotor flux linkage, T_e the electromagnetic torque, T_L the load torque, n_p the number of pole pairs, ω_e the rotor electrical speed, ω_r the rotor speed, $\omega_e = n_p \times \omega_r$, and J the moment of inertia. In this paper, the impact of saliency can be ignored for the SPMSM control strategy, i.e., $L_d = L_q = L_s$.

B. ERROR SYSTEM CONSTRUCTION AND IMPROVED ADAPTIVE LAW

A stator current-based MRAS is applied as estimator for the required variable estimation, in which the difference between the measured stator current and the estimated current obtained from the adjustable model is used to produce the

error signal. Hence, a current error system should be constructed firstly. Based on the mathematical model, the current differential equation in matrix form is derived as

$$p\begin{bmatrix} i_d + \dfrac{\psi_f}{L_s} \\ i_q \end{bmatrix} = \begin{bmatrix} -\dfrac{R_s}{L_s} & \omega_e \\ -\omega_e & -\dfrac{R_s}{L_s} \end{bmatrix} \begin{bmatrix} i_d + \dfrac{\psi_f}{L_s} \\ i_q \end{bmatrix} + \begin{bmatrix} \dfrac{u_d}{L_s} + \dfrac{R_s\psi_f}{L_s^2} \\ \dfrac{u_q}{L_s} \end{bmatrix} \tag{5}$$

where p is the differential operator. Some definitions are made as: $\boldsymbol{A} = \begin{bmatrix} -\frac{R_s}{L_s} & \omega_e \\ -\omega_e & -\frac{R_s}{L_s} \end{bmatrix}$, $\boldsymbol{i_s'} = \begin{bmatrix} i_d' & i_q' \end{bmatrix}^T = \begin{bmatrix} i_d + \frac{\psi_f}{L_s} & i_q \end{bmatrix}^T$, $\boldsymbol{u_s'} = \begin{bmatrix} \frac{u_d}{L_s} + \frac{R_s\psi_f}{L_s^2} & \frac{u_q}{L_s} \end{bmatrix}^T$. Then, Eq. (5) can be simplified as

$$p\boldsymbol{i_s'} = \boldsymbol{A}\boldsymbol{i_s'} + \boldsymbol{u_s'} \tag{6}$$

Substituting the estimated speed $\hat{\omega}_e$ with the actual speed ω_e into (5), it will get

$$p\hat{\boldsymbol{i}}_{\boldsymbol{s}}' = \hat{\boldsymbol{A}}\hat{\boldsymbol{i}}_{\boldsymbol{s}}' + \boldsymbol{u_s'} \tag{7}$$

where $\hat{\boldsymbol{i}}_{\boldsymbol{s}}' = \begin{bmatrix} \hat{i}_d' \\ \hat{i}_q' \end{bmatrix} = \begin{bmatrix} \hat{i}_d + \frac{\psi_f}{L_s} \\ \hat{i}_q \end{bmatrix}$ and $\hat{\boldsymbol{A}} = \begin{bmatrix} -\frac{R_s}{L_s} & \hat{\omega}_e \\ -\hat{\omega}_e & -\frac{R_s}{L_s} \end{bmatrix}$. The key point to design a model reference adaptive system is the choice of reference model and adjustable model. Since the state matrix $\hat{\boldsymbol{A}}$ contains the estimated speed, Eq. (7) is chosen as the adjustable model to produce the estimated current. The SPMSM is chosen as reference model in this case, while the actual current can be measured by the current sensor. Subtracting (6) from (7), the stator error equation can be written as

$$p\boldsymbol{e} = \boldsymbol{A}\boldsymbol{e} - \left(\hat{\omega}_e - \omega_e\right)\boldsymbol{E}\begin{bmatrix} \hat{i}_d' \\ \hat{i}_q' \end{bmatrix} \tag{8}$$

where the stator current error $\boldsymbol{e} = \boldsymbol{i_s'} - \hat{\boldsymbol{i}}_{\boldsymbol{s}}'$, the estimated speed error $\Delta\omega_e = \omega_e - \hat{\omega}_e$, and $\boldsymbol{E} = \begin{bmatrix} 0 & 1 \\ -1 & 0 \end{bmatrix}$. From the current error based on (8), the system with current error as state variable can be obtained as

$$\begin{cases} p\boldsymbol{e} = \boldsymbol{A}\boldsymbol{e} - \boldsymbol{W} \\ \boldsymbol{V} = \boldsymbol{C}\boldsymbol{e} \end{cases} \tag{9}$$

where $\boldsymbol{W} = \left(\hat{\omega}_e - \omega_e\right)\boldsymbol{E}\hat{\boldsymbol{i}}_{\boldsymbol{s}}'$, $\boldsymbol{C}$ is a linear compensation matrix. For the SPMSM, $\boldsymbol{C}$ can be selected as identity matrix for the working stability.

The typical structure of MRAS is depicted in Fig. 1, where the error system can be converted into a linear forward channel and a non-linear feedback channel. And V and W in (9) are the input and output of non-linear feedback channel, separately. Then the Popov's Hyper-Stability Theory is used to design an adaptive law.

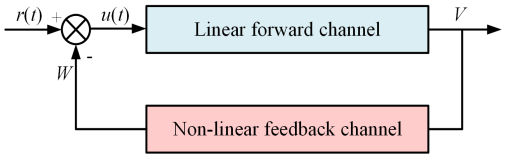

FIGURE 1. The typical structure of model reference adaptive system.

In the classical MRAS speed estimator, a PI controller is used as an adaptive law [9], which calculates the rotor speed based on the current error only produced by the electromagnetic model, as given by

$$\begin{aligned} \hat{\omega}_e &= k_i \int (\boldsymbol{Ce})^T \left(\boldsymbol{E}\hat{\boldsymbol{i}}_{\boldsymbol{s}}'\right) d\tau + k_p (\boldsymbol{Ce})^T \left(\boldsymbol{E}\hat{\boldsymbol{i}}_{\boldsymbol{s}}'\right) + \hat{\omega}_e(0) \\ &= \left(k_p + \frac{k_i}{s}\right)\left(i_d'\hat{i}'_q - i_q'\hat{i}'_d\right) + \hat{\omega}_e(0) \end{aligned} \tag{10}$$

where both k_p and k_i are the positive numbers. The initial value is usually set to 0.

In this paper, in order to further consider the impact of load disturbance on the dynamic performance of the system, the mechanical model in (4) is taken into account as a part of the proposed IAL-MRAS. One effective method to consider the mechanical model and suppress disturbance in speed sensed drives is the linear ESO, as expressed by

$$\begin{cases} \dot{\hat{\omega}}_e = \dfrac{n_p}{J}\left(T_e - \hat{T}_L\right) \\ \dot{\hat{T}}_L = -\left(\beta_1 + \dfrac{\beta_2}{s}\right) e_\omega \end{cases} \tag{11}$$

where $e_\omega = \omega_e - \hat{\omega}_e$ is the speed estimation error, β_1 and β_2 are the observer gains. However, this observer is only effective in the speed sensed conditions, because the actual speed is needed to calculate the error. From the linear ESO, the estimated load torque can be written as

$$\hat{T}_L = -\left(\frac{J}{n_p}\frac{d\hat{\omega}_e}{dt} - T_e\right) \tag{12}$$

As seen from (12), it is concluded that one definite relationship exists between the estimated load torque and the estimated speed. To estimate the load torque in the sensorless drives, the speed estimation error in linear ESO is replaced by the current error obtained by the electromagnetic model. Once $\hat{T}_L$ is determined using stator current error as (10), $\hat{\omega}_e$ can be calculated based on this definite relationship. Based on this idea, the adaptive law for $\hat{T}_L$ is chosen as

$$\hat{T}_L = -\left(k_p + \frac{k_i}{s}\right)\left(i_d'\hat{i}'_q - i_q'\hat{i}'_d\right) \tag{13}$$

Next, substituting (13) into (11) yields

$$\hat{\omega}_e = \frac{n_p}{Js}\left[\left(k_p + \frac{k_i}{s}\right)\left(i_d'\hat{i}'_q - i_q'\hat{i}'_d\right) + T_e\right] \tag{14}$$

where both k_p and k_i are the positive numbers. By integrating the estimated speed, the estimated rotor position is achieved as

$$\hat{\theta}_e = \int \hat{\omega}_e dt \tag{15}$$

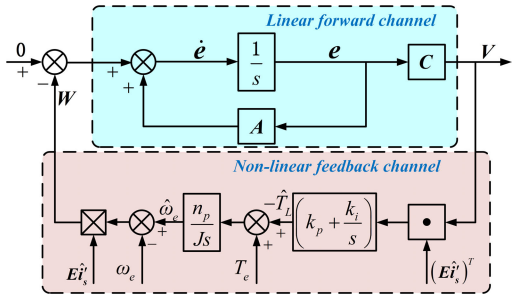

FIGURE 2. Model of the error system.

The obtained estimated speed and rotor position are used in the adjustable model in (7) as changeable parameters. Because of the closed-loop correction capability of MRAS, the initial value of the integral does not affect the steady state estimation results. In the IAL as shown in (13) and (14), the classical MRAS is contained, while the load torque introduced by the mechanical model is also estimated. In comparison with the classical MRAS, the PI adaptive law for speed estimation is replaced with a mechanical model based adaptive law, in which both the speed and load torque can be obtained in this new structure. The load torque obtained by IAL-MRAS contains disturbance information during the motor operation, which is beneficial to understand the operation status and adjust the system timely. Hence, IAL-MRAS as shown in Eqs. (13) and (14) are adopted in this paper to estimate the speed and load torque simultaneously. The model of error system in (9) can be presented with the obtained IAL, as shown in Fig. 2.

C. LINEARIZED MODEL OF THE IAL-MRAS

Whether the tuning of the adaptive law parameters or the further analysis for the system, it is difficult to deal with the non-linear feedback channel. Therefore, linearizing the error system as shown in Fig. 2 is necessary in this study. With the linearized model of IAL-MRAS, the transfer function can be used to analyze the system.

Taking the actual speed as the input and the estimated speed as the output, the error system can be linearized to obtain a block diagram, while the torque is processed as a disturbance signal. The linearized error system is presented in Fig. 3. It can be inferred in Fig. 3 that the variable y is a function of the estimation error e_ω, and the transfer function $G(s)$ between the variable y and the estimation error e_ω is calculated by

$$\begin{aligned} G(s) &= \frac{y(s)}{e_\omega(s)} = \left(\boldsymbol{E}\hat{\boldsymbol{i}}_{\boldsymbol{s}}^{\prime}\right)^T \left[\boldsymbol{C}(s\boldsymbol{I}-\boldsymbol{A})^{-1}\right]\left(\boldsymbol{E}\hat{\boldsymbol{i}}_{\boldsymbol{s}}^{\prime}\right) \\ &= \left[\left(\hat{i}_d + \frac{\psi_f}{L_s}\right)^2 + \hat{i}_q^2\right]\left(s + \frac{R_s}{L_s}\right) \Bigg/ \left[\left(s + \frac{R_s}{L_s}\right)^2 + \omega_e^2\right] \end{aligned} \tag{16}$$

Then the transfer function between torque and speed can be written as

$$T_e = T_L + \frac{Js\omega_e}{n_p} \tag{17}$$

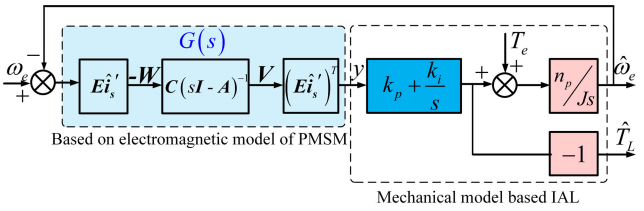

FIGURE 3. Structure diagram of the linearized error system.

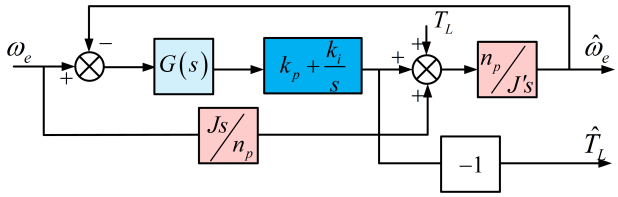

FIGURE 4. Linearized model of IAL-MRAS.

Substituting T_e in Fig. 3 by the relationship expressed as (17), the linearized model of IAL-MRAS can be gotten as shown in Fig. 4. Considering that the equivalent moment of inertia for the actual system varies with different loading operations, the moment of inertia J' used in the IAL may be different from the real value J. Therefore, they are presented in different forms in Fig. 4.

According to Fig. 4, the estimated rotor speed and load torque can be obtained by

$$\begin{cases} \hat{\omega}_r = \dfrac{J/J' + G_o(s)}{1 + G_o(s)}\omega_r + \dfrac{1}{1 + G_o(s)}\dfrac{1}{J's}T_L \\ \hat{T}_L = \dfrac{(J - J')\,G_o(s)}{1 + G_o(s)}s\omega_r + \dfrac{G_o(s)}{1 + G_o(s)}T_L \end{cases} \tag{18}$$

where $G_o(s) = n_p G(s)\frac{(k_p s + k_i)}{J's^2}$ is the open-loop transfer function of IAL-MRAS. It can be seen from (18) that, according to the Final Value Theorem, the estimated result converges to the actual value at steady state, even if the inertia in the IAL is different from the actual value. Hence, it does not make any difference on the accuracy at steady state. When $J' = J$, the dynamic error of the estimated parameters will only be related to the change of the load itself. At this time, the system will obtain the most ideal dynamic performance.

III. SENSORLESS CONTROL BASED ON THE IAL-MRAS

A. COMPOSITE SPEED CONTROLLER BASED ON IAL-MRAS

The main key performance indexes for the speed controller design are the speed tracking response and the load disturbance rejection ability. Besides, the extra dynamic between the estimated and actual values makes it more complex for the sensorless drives. Fortunately, the estimated disturbance based control method exhibits good performance against the load disturbance, and has been employed in many industry systems. Using the load torque estimated by IAL-MRAS, a composite speed controller with strong disturbance rejection ability while only P gain needs to be tuned is proposed in this section.

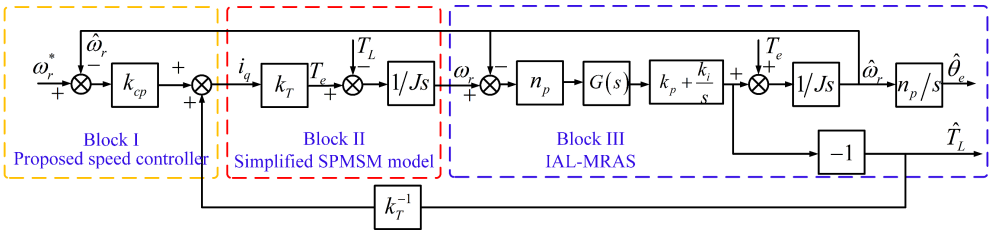

FIGURE 5. Sensorless control scheme based on the proposed speed controller.

Generally, the mechanical time constant of PMSM is much greater than the electrical time constant in actual drive system. Therefore, when focusing on the speed controller, the dynamic process of the current response can be ignored. That is to say, it is approximately considered that the d-q axis current can follow the reference value in real time.

To decouple the speed and current loops, $i_d = 0$ control strategy is used in this paper. For $i_d = 0$ strategy, the electromagnetic torque can be expressed as

$$T_e = \frac{3}{2} n_p \psi_f i_q = k_T i_q \tag{19}$$

where k_T is named as torque coefficient. Combining (19) and the mechanical motion equation, a simplified model of the SPMSM is obtained as shown in Block II, Fig. 5.

With the IAL-MRAS in this paper, both the speed and the load torque is obtained simultaneously. Thus, the estimated load torque can be feedforwarded proportionally to the q-axis current, which provides the compensation signal when the load is disturbed. Hence, a speed controller can be designed as

$$i_q^* = k_{cp} \left(\omega_r^* - \hat{\omega}_r \right) + \hat{T}_L \Big/ k_T \tag{20}$$

It can be concluded from (20) that when the system is disturbed, the item containing the estimated load torque will change to adjust the q-axis current at first, reducing the fluctuation that may be caused to the speed. The final sensorless control scheme based on the proposed speed controller with linearized IAL-MRAS and simplified SPMSM model is shown in Fig. 5.

It is worth noting that the estimated load torque must be equal to its actual value in the steady state, otherwise the integration process will continue and the speed cannot reach the steady value. Therefore, because of the integral gain used in the IAL-MRAS, it can ensure that the final estimated value has no steady state error. Compared to the conventional methods, the speed controller proposed in this paper can provide greater convenience for its parameter tuning, while the PI gains in speed controller are usually difficult to determine in practice. Moreover, it can enhance the robustness of sensorless drives by feedforwarding the estimated load torque into the speed controller.

B. I-f STARTUP STRATEGY

It should be noted that the IAL-MRAS is based on the back EMF model that suffers from poor zero-low speed performance. To achieve the sensorless control in the full speed range, other methods suitable for zero-low speed range should be combined with the IAL-MRAS. Nowadays, V/F scalar control is widely used in many applications due to its simple control structure. However, because of the absence of current regulation, this method has the disadvantages of high current and torque ripples [27]. In this paper, the current closed-loop I-f control strategy is adopted as a startup strategy, while the motor can be accelerated from standstill to a certain speed by tracking a frequency command. And then the control strategy will switch to IAL-MRAS at suitable speed.

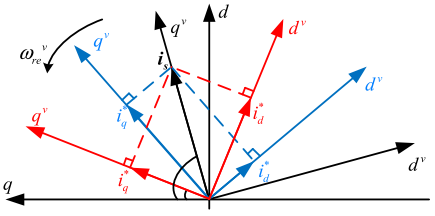

FIGURE 6. Phase relationship between d-q and d^v-q^v in the transition process.

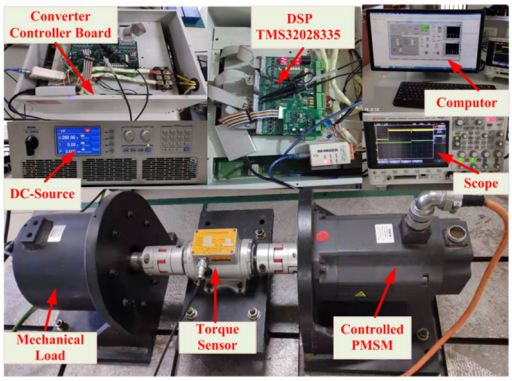

FIGURE 7. The experimental test platform.

The rotor position used in I-f control is obtained by integrating the given frequency, so it is also a speed open-loop control strategy. In order to distinguish the actual rotor coordinate system from this virtual one, they are defined as $d-q$ and d^v-q^v respectively. For a smooth transition, a certain method is needed to guarantee that these two coordinate systems can gradually coincide with each other. In [28], a smooth transition strategy is proposed by redistributing the reference value of d^v-q^v axis currents as described in (21), and these two coordinate systems will approach until the transition condition is satisfied.

$$\begin{cases} i_d^* (t) = i_s^* (t_0) \sin \left[m (t - t_0) \right] \\ i_q^* (t) = i_s^* (t_0) \cos \left[m (t - t_0) \right] \end{cases} \tag{21}$$

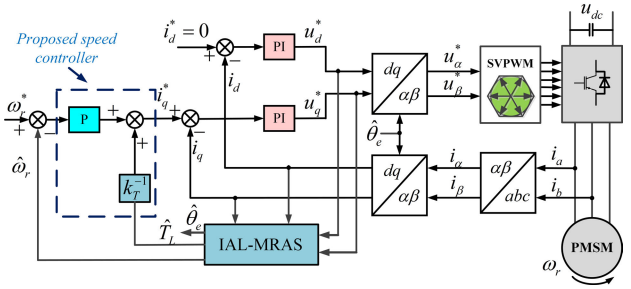

FIGURE 8. Diagram of the proposed sensorless control scheme based on the IAL-MRAS.

TABLE 1. Main parameters of the PMSM.

Quantity	Symbol	Value	Unit
Rated power	P_N	3	kW
Number of pole pairs	n_p	3	-
Flux linkage	ψ_f	0.35	Wb
Stator resistance	R_s	0.8	Ω
Stator inductance	L_s	5	mH
Rated torque	T_N	14	Nm
Rated speed	n_N	2000	rpm
Rated current	I_N	7	A
Moment of inertia	J	3.78×10^{-4}	kg·m^2

where m is the slope for angle adjustment, $m > 0$. The phase relationship between $d-q$ and d^v-q^v in transition is shown in Fig. 6. When i_q^* is decreased, in order to balance the load torque as before, the q^v axis will then rotate towards the q axis. The aforementioned method is used for the transition in this paper.

IV. SIMULATION AND EXPERIMENTAL RESULTS

To verify the feasibility and improvements of the proposed method, numerical simulations and experimental tests are implemented. Main parameters used in the validation are presented in Table 1, which come from one prototyped 3kW PMSM platform as shown in Fig. 7. The block diagram of the sensorless control based on IAL-MRAS is shown in Fig. 8, in which the general field oriented control(FOC) is used as the basic control scheme.

A. SIMULATION RESULTS AND DISCUSSIONS

Numerical simulation is used to determine the PI gains in IAL-MRAS, which is not convenient to be tuned in the experiment directly. By the trial and error method in simulation, the PI gains in (13) are finally set to 0.05 and 60. Fig. 9 depicts the estimation response under the speed variation, while the reference speed steps from 200 rpm to 400 rpm and the load torque is maintained at rated value. In the whole process, the estimated speed/position and load torque can track its actual value quickly. Meanwhile, the estimation performance to load torque variation is shown in Fig. 10. The reference speed is given as 200 rpm while a rated torque is suddenly applied to the system. It can be seen that the estimator can return steady state after an oscillation. Fig. 11 depicts the estimation performance under rated speed and load torque, where the proposed method can achieve accurate estimation

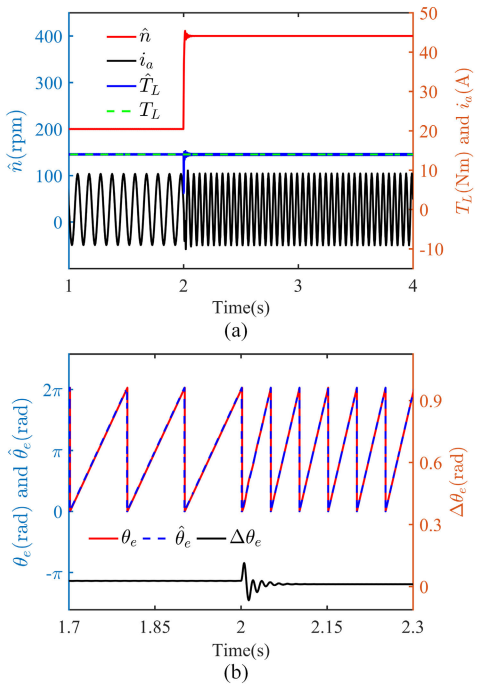

FIGURE 9. Simulated estimation performance under speed variation. (a) Estimated speed and torque. (b) Estimated position.

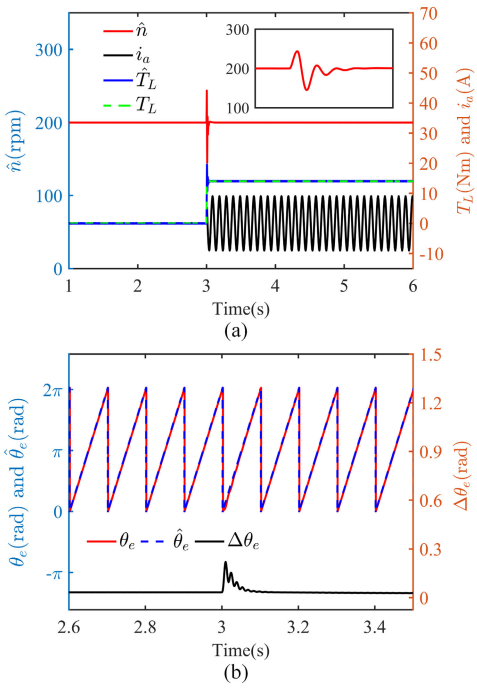

FIGURE 10. Simulated estimation performance under load torque variation. (a) Estimated speed and torque. (b) Estimated position.

of speed/position and load torque simultaneously under rated working conditions. Both working conditions can be used to illustrate the effectiveness of the proposed IAL-MRAS and the feasibility of PI gains in IAL-MRAS.

Based on the PI gains that have been well tuned, the stability of IAL-MRAS is analyzed by the root locus of the transfer function as defined in (18). Fig. 12 depicts the location of the

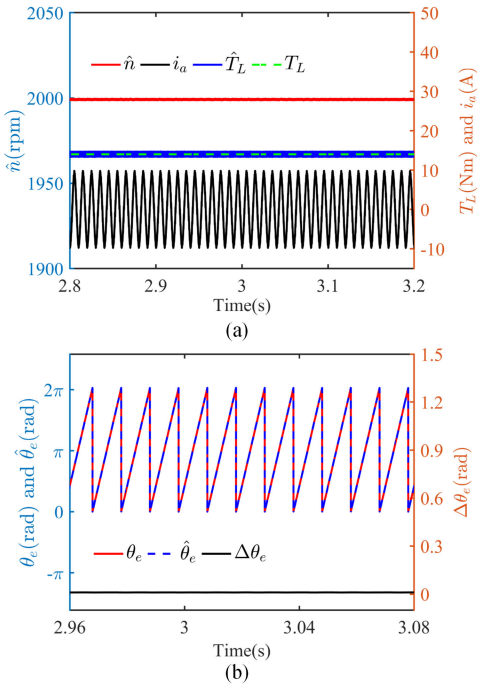

FIGURE 11. Simulated estimation performance under rated speed and load torque. (a) Estimated speed and torque. (b) Estimated position.

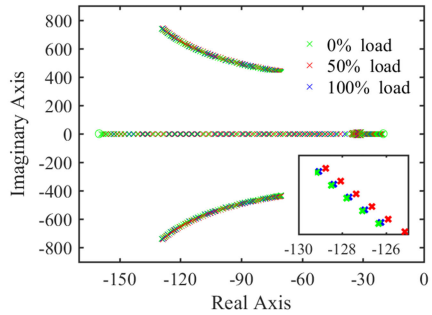

FIGURE 12. Pole placement for the transfer function of IAL-MRAS. ($\hat{\omega}_e = 0.05 \rightarrow 1p.u.$)

TABLE 2. Specific parameters in the control method.

Name	Value
PI gains of the current controller with (PI)	11 and 120
PI gains of the conventional speed controller with (PI)	0.15 and 1.2
P gain of the proposed speed controller with (P)	0.1
PI gains of the PDF speed controller with (PI)	0.1 and 2
PI gains of the improved adaptive law with (PI)	0.05 and 60

closed-loop poles and zeros under different load torque for the speed range $\hat{\omega}_e = 0.05 \rightarrow 1p.u.$ It can be seen that all the poles and zeros are located on the negative semi-axis of the real axis, indicating the proposed speed/position estimator is stable during $\hat{\omega}_e = 0.05 \rightarrow 1p.u.$

Fig. 13 (a) compares the step responses for the proposed speed controller and PI controller. The speed responses are obtained with different P gains in the speed controller, and the I gain in PI controller is given as 1.2 after many attempts, which is the optimal value with a better response. It can be seen that the proposed speed controller has a smaller settling

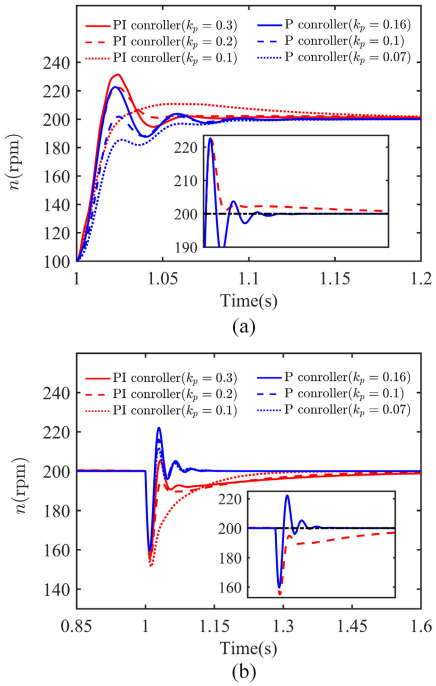

FIGURE 13. Performance comparison for PI controller and P controller. (a) Speed tracking ability. (b) Load disturbance rejection ability.

time for the same overshoot, which can improve the dynamic response of SPMSM drive. The ability to load disturbance rejection is shown in Fig. 13 (b), where a 6 Nm load is suddenly applied to the system, with the reference speed maintained at 200 rpm. It can be found that the proposed method has better drive performance, such as smaller speed dip and settling time. Based on the simulated response, the parameters for different speed controllers are further tuned for the nearly same current overshoot, so that a fair comparison can be achieved. Other optimized control parameters used in simulation are listed in Table 2, which are similar as those in experiments.

B. EXPERIMENTAL RESULTS AND DISCUSSIONS

The proposed method is verified in the test platform as shown in Fig. 7, which is controlled by a control board with one TMS320F28335 digital signal processor (DSP), and the three-phase pulse width modulation (PWM) conducts alternative current for the PMSM drive. The carrier frequency of the PWM inverter is set to 5 kHz. And the sampling period of analogue inputs, including stator current and DC voltage is 200 us. Main drive indexes are converted to analog signals using D/A converter and analyzed using digital oscilloscope.

1) CASE-1: *I-f* STARTUP AND SMOOTH TRANSITION TO IAL-MRAS

In order to solve the problem of inaccurate position estimation under low speed operation based on IAL-MRAS, the working states starting up with *I-f* strategy and transition to IAL-MRAS are adopted in this paper. A preposition is

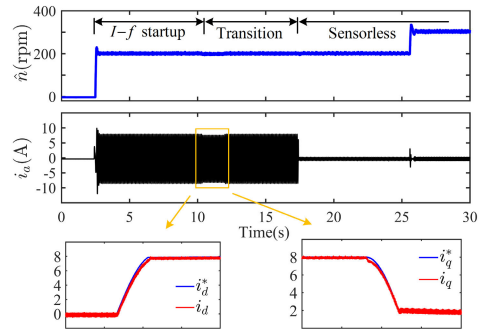

FIGURE 14. The startup and smooth transition to IAL-MRAS.

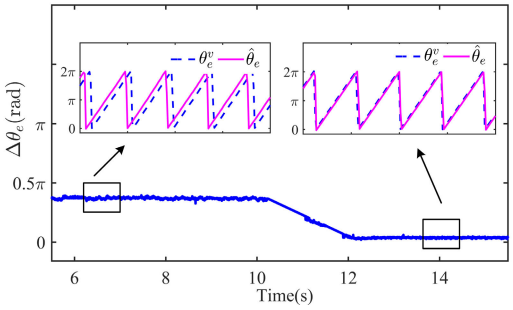

FIGURE 15. The phase relationship during transition process.

carried out before startup, which is achieved by applying DC current to stator winding to make the d-axis of rotor coincide with the A-axis of stator winding. Fig. 14 shows the speed and stator current responses during the whole process from startup to transition. The reference frequency for *I-f* strategy is set to 10 Hz (200 rpm), which is sufficient for the IAL-MRAS to realize accurate position estimation. Because the absence for speed regulation in *I-f* strategy, the given value of q^v-axis current is set to 8 A and the rising speed of frequency is set to 55 Hz/s after many attempts to ensure that the system has a fast enough startup process with a less speed overshoot. It can be observed from Fig. 15 that if the reference value of d-q axis current is changed as (21), then the virtual rotor position θ_e^v in *I-f* strategy will get close to the real one. As a result, a smooth transition with little current and speed fluctuations can be achieved. In the current changing transition period, an important parameter to set up is the slope for angle adjustment m, which determines the stability and settling time during the transition. By adjusting m according to the response, its final value is set to 0.8. Once the transition is completed, the reference speed steps to 300 rpm, and the system can run stably in the closed-loop control.

To further validate the sensorless control performance in a wider speed range, the system response from 200 rpm to 2000 rpm is shown in Fig. 16, where the reference speed is set as a ramp command. It can be seen that the estimated speed can track the actual speed well in the whole speed range. In Fig. 16, the phase current becomes larger with the rising speed, and the system works at rated speed and load torque after reaching the steady state. The results confirm the effectiveness of the proposed sensorless control method in different working conditions.

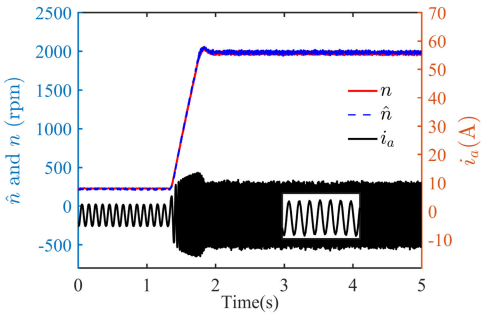

FIGURE 16. The system response from 200 rpm to 2000 rpm under a ramp command.

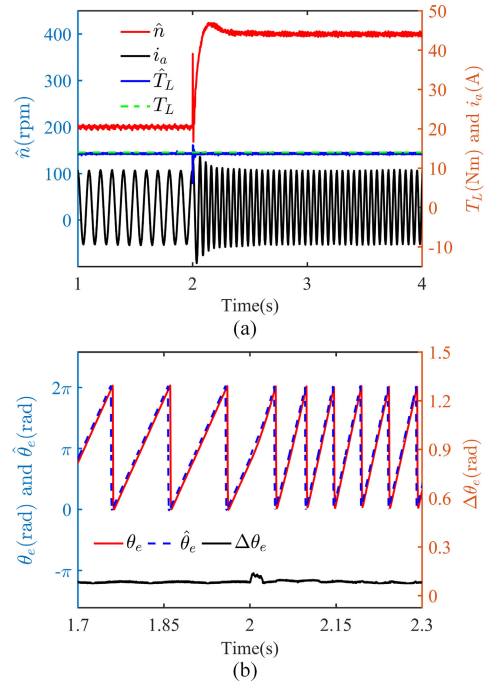

FIGURE 17. Response to a speed step from 200 rpm to 400 rpm at 14 Nm. (a) Estimated speed and torque. (b) Estimated position.

2) CASE-2: PERFORMANCE ANALYSIS BASED ON IAL-MRAS

In order to ensure the effectiveness of IAL-MRAS under different working states, the results of estimated rotor position and load torque by IAL-MRAS under different speed ranges are shown in Figs. 17-21, respectively. The estimation error of rotor position in all figures is taken the remainder of 2π to avoid periodic pulses. And the actual rotor position obtained by the sensor is only used to compare with its estimated value.

To validate the dynamic and steady state performance of IAL-MRAS, the response under a speed step change from 200 rpm to 400 rpm is illustrated in Fig. 17, while the load torque is maintained at the rated torque. It can be seen that the IAL-MRAS is successful in keeping the estimated speed tracking closely the reference value, and the estimated torque is approximately equal to the actual load torque. When the reference speed changes, the estimated value can follow the actual one after a short transient process. Meanwhile, the response under a rated torque step change at

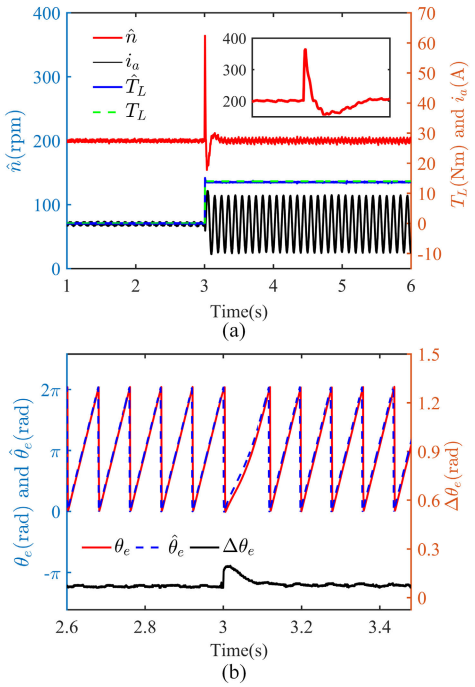

FIGURE 18. Response to a load step from 0 Nm to 14 Nm at 200 rpm. (a) Estimated speed and torque. (b) Estimated position.

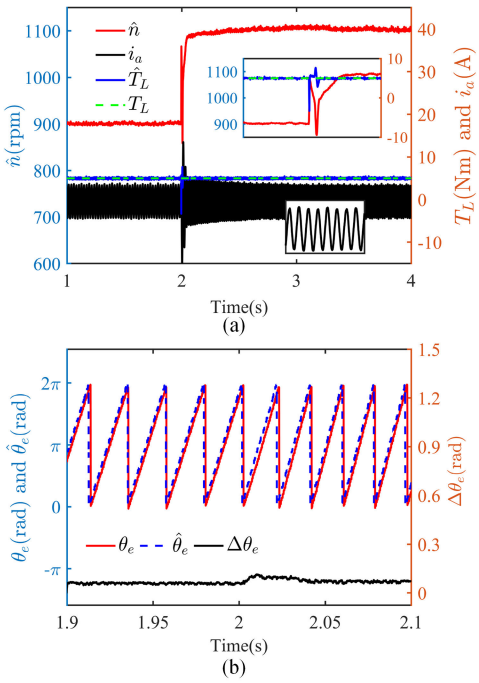

FIGURE 19. Response to a speed step change from 900 rpm to 1100 rpm at 5 Nm. (a) Estimated speed and torque. (b) Estimated position.

200 rpm is presented in Fig. 18, in which the proposed method can also estimate the rotor position and load torque simultaneously. Once the rated load torque is applied to the system, the estimated speed can quickly recover to steady state after a short-term oscillation, so that the error of position estimation is not large enough during the whole process. The dynamic responses at 900 rpm are presented in Figs.19 and 20, where

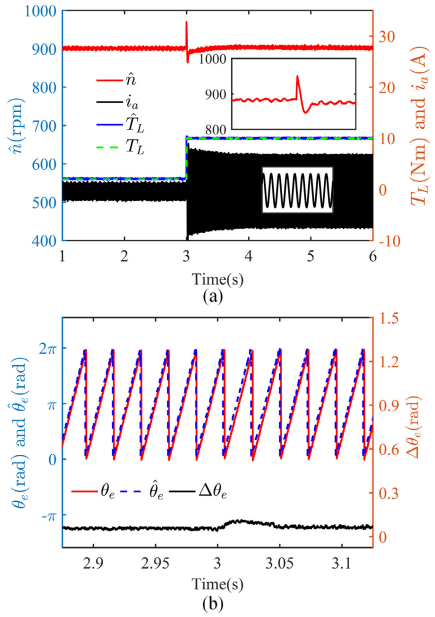

FIGURE 20. Response to a load step change from 2 Nm to 10 Nm at 900 rpm. (a) Estimated speed and torque. (b) Estimated position.

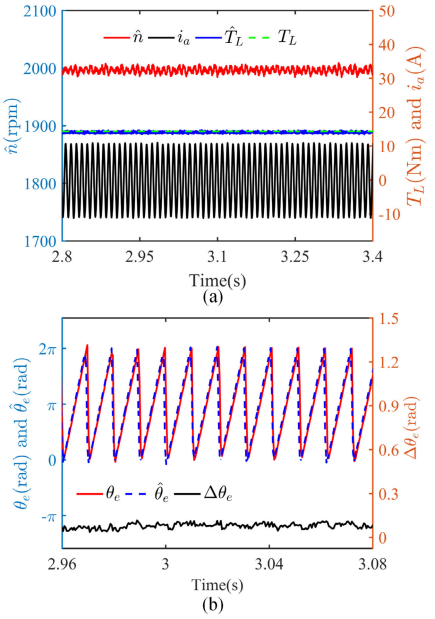

FIGURE 21. Estimation performance under the rated speed and load torque. (a) Estimated speed and torque. (b) Estimated position.

both the rotor position and load torque can track their actual value as those shown in the lower speed. Fig. 21 shows the estimated performance under the rated working condition, confirming the estimation effectiveness of IAL-MRAS under various working states.

3) CASE-3: PERFORMANCE EVALUATION OF THE DRIVE SYSTEM

Firstly, in order to confirm the dynamic and steady-state performance of the proposed speed controller in sensorless control, the speed response with different k_p parameters is

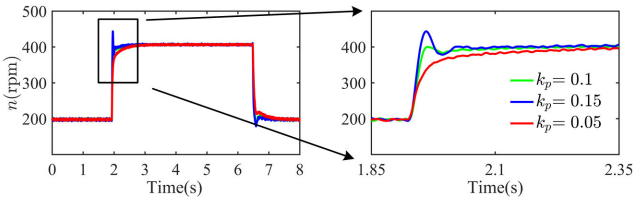

FIGURE 22. Speed step response with the proposed method.

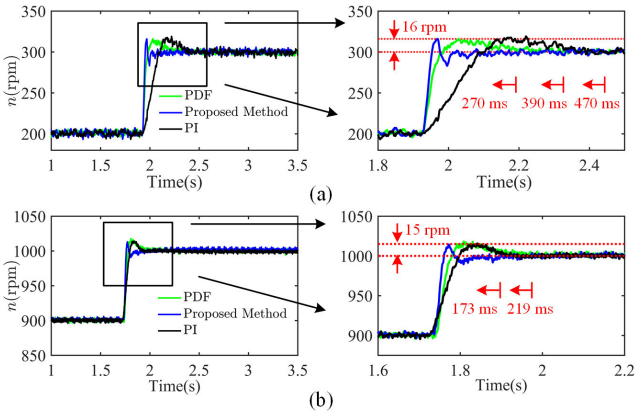

FIGURE 23. Step response of PI, PDF [17] and the proposed method. (a) From 200 rpm to 300rpm under 10 Nm. (b) From 900 rpm to 1000rpm under 5 Nm.

depicted in Fig. 22, where the reference speed steps from 200 rpm to 400 rpm and finally returns to 200 rpm. It can be seen that with the proposed speed controller, the actual speed can track the reference value well for step changes. Moreover, the speed response is adjusted only by k_p, which means only one parameter needs to be tuned in practice. The speed tracking ability under speed step change for PI controller, pseudo-derivative feedback (PDF) controller [17] and the proposed controller is depicted in Fig. 23, while the overshoot under different responses is adjusted to be nearly the same. It can be found that the proposed controller has smaller settling time in dynamic process for a speed step change.

The disturbance rejection ability under the PI, PDF [17] and the proposed controller is compared at 400 rpm and 1000 rpm with a step of load torque from 4 Nm to 10 Nm. The gains in different speed controllers are tuned for a fair comparison with a limitation of ±20A, while the current loop gains are the same in all methods. Figs. 24 and 25 show the speed and q-axis current responses for different speed controllers. It can be obtained from Fig. 24 (a) that speed dip and settling time under the PI, PDF [17], and the proposed controller are (59 rpm, 310 ms), (52 rpm, 223 ms), and (27 rpm, 111 ms), separately, while the current overshoot in different cases are tuned to be nearly the same for a fair comparison. In Fig. 24 (b), q-axis current in proposed controller can get a faster response once the load is changed due to the load torque estimation by IAL-MRAS, which can reduce the speed dip and settling time. And q-axis current plays a regulatory role only when the rotor speed has changed in other controllers. The similar dynamic response is shown in Fig. 25 for the

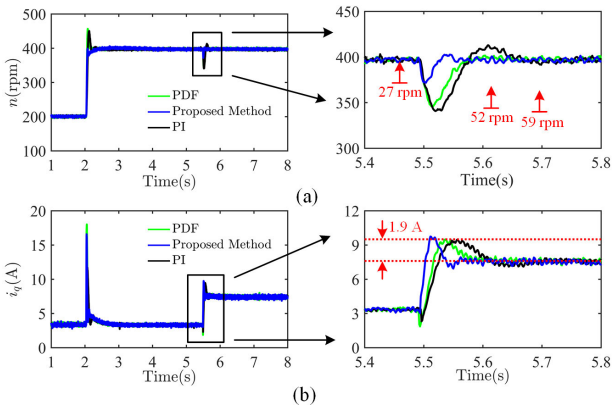

FIGURE 24. The load disturbance rejection ability of PI, PDF [17] and the proposed method at 400 rpm. (a) Speed. (b) q-axis current.

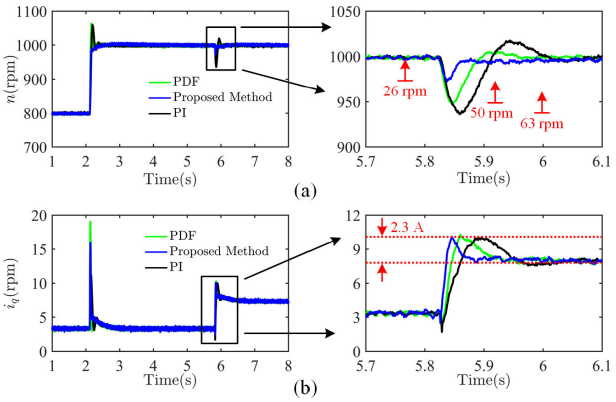

FIGURE 25. The load disturbance rejection ability of PI, PDF [17] and the proposed method at 1000 rpm. (a) Speed. (b) q-axis current.

reference speed at 1000 rpm. Hence, the $\hat{T}_L$ can play an important role in improving the dynamic performance.

In Fig. 26, the proposed speed controllers with P gain ($k_p = 0.12$, case 1), PI gains ($k_p = 0.12$, $k_i = 2$, case 2) and PI gains ($k_p = 0.12$, $k_i = 10$, case 3) are tested, respectively. It is worth noting that I gain is not necessary in the proposed controller, leading to a simplification in parameter tuning. The above results indicate that the proposed speed controller with feedforward compensation has a superior dynamic performance than other conventional methods in the sensorless drives.

4) CASE-4: PARAMETER SENSITIVITY ANALYSIS

As well known, it is difficult to get accurate parameters in practice due to the variations injected by noise or temperature. Unfortunately, the d-q axis currents used in the IAL as shown in (13) and (14) rely on machine parameters closely. Thus, it is necessary to evaluate the parameter sensitivity of IAL-MRAS in this work. When the reference speed is given as 400 rpm and the load torque is set as 4 Nm, the estimation error under different parameter variations is shown in Fig. 27, where the stator resistance R_s, stator inductances L_s are suddenly increased with a 150% magnitude, separately. From the experimental results, it is shown that the parameter variation has little effect on the estimated load torque. On the other hand, the sudden change of parameters has some influence on

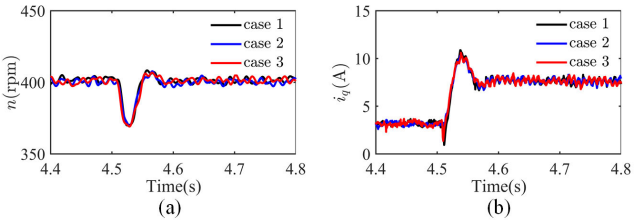

FIGURE 26. Effects of I gain in the proposed speed controller. (a) Speed. (b) q-axis current.

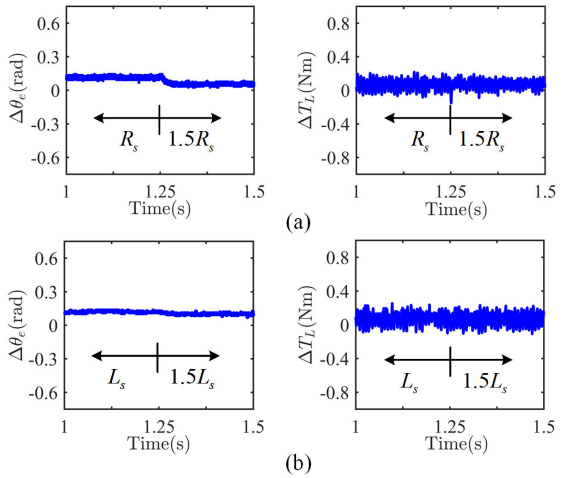

FIGURE 27. Parameter sensitivity analysis of the IAL-MRAS. (a) R_S mismatch. (b) L_S mismatch.

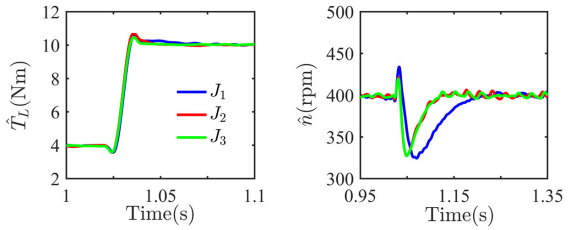

FIGURE 28. Dynamic performance of the IAL-MRAS when the moment of inertia mismatches. ($J_1 = 3.78 \times 10^{-4}\text{kg}\cdot\text{m}^2$, $J_2 = 6 \times 10^{-4}\text{kg}\cdot\text{m}^2$, $J_3 = 1 \times 10^{-4}\text{kg}\cdot\text{m}^2$).

the estimated rotor position, especially the stator resistance. However, the system can still run stably after the parameter variation, which means the proposed method is robust to parameter variation.

Fig. 28 studies the influence of the moment of inertia on the estimated results, where three different values are used in the IAL, respectively. To compare the estimated results in the dynamic process, a load torque step change from 4 Nm to 10 Nm at 400 rpm is applied to the system. It can be observed in Fig. 28 that the difference between them is mainly reflected in the dynamic adjustment process. However, after a transient vibration, the result can track the actual value gradually. And the three curves are almost identical at steady state, without affecting the accuracy of steady state.

V. CONCLUSION

In this paper, an IAL-MRAS is proposed by incorporating the mechanical and electromagnetic model to estimate the load torque and speed simultaneously. Based on the IAL-MRAS, both the speed/position estimator and the speed controller with load torque feedforward compensation scheme are designed in a systematic manner to significantly enhance the dynamic performance for an SPMSM sensorless drive. Besides, only P gain needs to be tuned in the proposed speed controller, which would bring great convenience to the practical application of the drive system. To realize wide-speed-range sensorless control, a hybrid strategy integrating with both IAL-MRAS and *I-f* starting method is adopted. Comprehensive numerical simulation and experimental results, under different load disturbances, operation speeds, and machine parameters variation, have confirmed that the proposed method is with strong capability to improve the dynamic performance of SPMSM sensorless drives. In the next stage study, the online inductance identification techniques combined with the proposed sensorless algorithm will be fully investigated to improve the robustness ability to nonlinear factors, such as magnetic saturation, *etc*.

REFERENCES

[1] A. K. Junejo, W. Xu, C. Mu, M. M. Ismail, and Y. Liu, "Adaptive speed control of PMSM drive system based a new sliding-mode reaching law," *IEEE Trans. Power Electron.*, vol. 35, no. 11, pp. 12110–12121, Nov. 2020.
[2] G. Wang, M. Valla, and J. Solsona, "Position sensorless permanent magnet synchronous machine drives—A review," *IEEE Trans. Ind. Electron.*, vol. 67, no. 7, pp. 5830–5842, Jul. 2020.
[3] J. Liu, T. A. Nondahl, P. B. Schmidt, S. Royak, and M. Harbaugh, "Rotor position estimation for synchronous machines based on equivalent EMF," *IEEE Trans. Ind. Appl.*, vol. 47, no. 3, pp. 1310–1318, May 2011.
[4] H. Kim, J. Son, and J. Lee, "A high-speed sliding-mode observer for the sensorless speed control of a PMSM," *IEEE Trans. Ind. Electron.*, vol. 58, no. 9, pp. 4069–4077, Sep. 2011.
[5] D. Liang, J. Li, and R. Qu, "Sensorless control of permanent magnet synchronous machine based on second-order sliding-mode observer with online resistance estimation," *IEEE Trans. Ind. Appl.*, vol. 53, no. 4, pp. 3672–3682, Jul./Aug. 2017.
[6] Z. Chen, M. Tomita, S. Doki, and S. Okuma, "An extended electromotive force model for sensorless control of interior permanent-magnet synchronous motors," *IEEE Trans. Ind. Electron.*, vol. 50, no. 2, pp. 288–295, Apr. 2003.
[7] S. Bolognani, R. Oboe, and M. Zigliotto, "Sensorless full-digital PMSM drive with EKF estimation of speed and rotor position," *IEEE Trans. Ind. Electron.*, vol. 46, no. 1, pp. 184–191, Feb. 1999.
[8] Y. Jiang, W. Xu, C. Mu, J. Zhu, and R. Dian, "An improved third-order generalized integral flux observer for sensorless drive of PMSMs," *IEEE Trans. Ind. Electron.*, vol. 66, no. 12, pp. 9149–9160, Dec. 2019.
[9] W. Xu, Y. Jiang, C. Mu, and F. Blaabjerg, "Improved nonlinear flux observer-based second-order SOIFO for PMSM sensorless control," *IEEE Trans. Power Electron.*, vol. 34, no. 1, pp. 565–579, Jan. 2019.
[10] G. Yang and T.-H. Chin, "Adaptive-speed identification scheme for a vector-controlled speed sensorless inverter-induction motor drive," *IEEE Trans. Ind. Appl.*, vol. 29, no. 4, pp. 820–825, Jul. 1993.
[11] S. S. Badini and V. Verma, "A novel MRAS based speed sensorless vector controlled PMSM drive," in *Proc. 54th Int. Universities Power Eng. Conf. (UPEC)*, Sep. 2019, pp. 1–6.
[12] W. Zhifu, T. Qizhi, and Z. Chengning, "Speed identification about PMSM with MRAS," in *Proc. IEEE 6th Int. Power Electron. Motion Control Conf.*, May 2009, pp. 1880–1884.
[13] Z. Zhong, M. Jing, and J. Shen, "Full speed range sensorless control of permanent magnet synchronous motor with phased PI regulator-based model reference adaptive system," *Proc. Chin. Soc. Elect. Eng.*, vol. 38, no. 4, pp. 1203–1211, 2018.
[14] O. C. Kivanc and S. B. Ozturk, "Sensorless PMSM drive based on stator feedforward voltage estimation improved with MRAS multiparameter estimation," *IEEE/ASME Trans. Mechatronics*, vol. 23, no. 3, pp. 1326–1337, Jun. 2018.

[15] F. Qin, Y. He, and H. Jia, "Investigation of the sensorless control for PMSM based on a hybrid rotor position self-sensing approach," *Proc. Chin. Soc. Elect. Eng.*, vol. 27, no. 3, pp. 12–17, 2007.
[16] Q. Tang, D. Chen, and X. He, "Integration of improved flux linkage observer and I–f starting method for wide-speed-range sensorless SPMSM drives," *IEEE Trans. Power Electron.*, vol. 35, no. 8, pp. 8374–8383, Aug. 2020.
[17] K. K. Prabhakaran and A. Karthikeyan, "Electromagnetic torque-based model reference adaptive system speed estimator for sensorless surface Mount permanent magnet synchronous motor drive," *IEEE Trans. Ind. Electron.*, vol. 67, no. 7, pp. 5936–5947, Jul. 2020.
[18] X. Zhang and Z. Li, "Sliding-mode observer-based mechanical parameter estimation for permanent magnet synchronous motor," *IEEE Trans. Power Electron.*, vol. 31, no. 8, pp. 5732–5745, Aug. 2016.
[19] S.-M. Yang and Y.-J. Deng, "Observer-based inertial identification for auto-tuning servo motor drives," in *Proc. 40th IAS Annu. Meeting Conf. Rec. Ind. Appl. Conf.*, Oct. 2005, pp. 968–972.
[20] R. Dian, W. Xu, J. Zhu, D. Hu, and Y. Liu, "An improved speed sensorless control strategy for linear induction machines based on extended state observer for linear metro drives," *IEEE Trans. Veh. Technol.*, vol. 67, no. 10, pp. 9198–9210, Oct. 2018.
[21] H. H. Choi, N. T.-T. Vu, and J.-W. Jung, "Digital implementation of an adaptive speed regulator for a PMSM," *IEEE Trans. Power Electron.*, vol. 26, no. 1, pp. 3–8, Jan. 2011.
[22] S. Li and Z. Liu, "Adaptive speed control for permanent-magnet synchronous motor system with variations of load inertia," *IEEE Trans. Ind. Electron.*, vol. 56, no. 8, pp. 3050–3059, Aug. 2009.
[23] W. Xu, A. K. Junejo, Y. Liu, and M. R. Islam, "Improved continuous fast terminal sliding mode control with extended state observer for speed regulation of PMSM drive system," *IEEE Trans. Veh. Technol.*, vol. 68, no. 11, pp. 10465–10476, Nov. 2019.
[24] G. Zhang, G. Wang, B. Yuan, R. Liu, and D. Xu, "Active disturbance rejection control strategy for signal injection-based sensorless IPMSM drives," *IEEE Trans. Transport. Electrific.*, vol. 4, no. 1, pp. 330–339, Mar. 2018.
[25] L. Yubo and W. Xudong, "Speed global integral sliding mode control with a load sliding mode observer for PMSM," *IEICE Electron. Exp.*, vol. 15, no. 6, 2018, Art. no. 20171270.
[26] L. Harnefors and M. Hinkkanen, "Stabilization methods for sensorless induction motor drives—A survey," *IEEE J. Emerg. Sel. Topics Power Electron.*, vol. 2, no. 2, pp. 132–142, Jun. 2014.
[27] Z. Wang, K. Lu, and F. Blaabjerg, "A simple startup strategy based on current regulation for back-EMF-based sensorless control of PMSM," *IEEE Trans. Power Electron.*, vol. 27, no. 8, pp. 3817–3825, Aug. 2012.
[28] J. Liu, F. Xiao, Z. Mai, S. Gao, and X. Yu, "Hyper position-sensorless control scheme for PMSM based on combination of IF control and sliding mode observer," *Trans. China Electrotech. Soc*, vol. 33, no. 4, pp. 919–929, 2018.

YIRONG TANG (Student Member, IEEE) received the B.E. degree in electrical engineering from Huazhong University of Science and Technology, Wuhan, China, in 2020, where he is currently pursuing the Ph.D. degree with the State Key Laboratory of Advanced Electromagnetic Engineering and Technology.

His research interests include advanced control methods for permanent magnet synchronous machines and linear induction machines and drives.

WEI XU (Senior Member, IEEE) received the double B.E. and M.E. degrees in electrical engineering from Tianjin University, Tianjin, China, in 2002 and 2005, respectively, and the Ph.D. degree in electrical engineering from the Institute of Electrical Engineering, Chinese Academy of Sciences, in 2008.

From 2008 to 2012, he was a Postdoctoral Fellow with the University of Technology Sydney, a Vice Chancellor Research Fellow with the Royal Melbourne Institute of Technology, and Japan Science Promotion Society Invitation Fellow with Meiji University. Since 2013, he has been a Full Professor with the State Key Laboratory of Advanced Electromagnetic Engineering, Huazhong University of Science and Technology, China. He has more than 110 articles accepted or published in IEEE journals, two edited books published by Springer Press, one monograph published by China Machine Press, and more than 150 invention patents granted or in pending, all in the related fields of electrical machines and drives. His research interests include design and control of linear/rotary machines. He is a fellow of the Institute of Engineering and Technology (IET). He will serve as the General Chair for the 2021 International Symposium on Linear Drives for Industry Applications (LDIA 2021) and the 2023 IEEE International Conference on Predictive Control of Electrical Drives and Power Electronics (PRECEDE 2023) in Wuhan, China, respectively. He has served as an Associate Editor for several leading IEEE TRANSACTIONS and journals, such as IEEE TRANSACTIONS ON INDUSTRIAL ELECTRONICS, IEEE TRANSACTIONS ON VEHICULAR TECHNOLOGY, and IEEE TRANSACTIONS ON ENERGY CONVERSION.

YI LIU (Senior Member, IEEE) received the B.E. and M.E. degrees in automation and control engineering from Wuhan University of Science and Technology, Wuhan, China, in 2004 and 2007, respectively, and the Ph.D. degree in mechatronic engineering from Huazhong University of Science and Technology, Wuhan, in 2016.

From March 2016 to June 2016, he was a Senior Research and Development Engineer at the Fourth Academy of China Aerospace Science and Industry Group, Wuhan. From July 2016 to October 2019, he was a Postdoctoral Research Fellow at the State Key Laboratory of Advanced Electromagnetic Engineering and Technology, Huazhong University of Science and Technology, where he has been a Lecturer, since January 2020. His current research interests include multi-port electrical machines and drive systems. He has received the Best Paper Award from IEEE TRANSACTIONS ON ENERGY CONVERSION, in 2020. He is the Vice Chair for IEEE IES Wuhan Chapter. He is an Associate Editor for IEEE TRANSACTIONS ON INDUSTRY APPLICATIONS.

DINGHAO DONG (Graduate Student Member, IEEE) received the B.E. degree in electrical engineering from Wuhan University, Wuhan, China, in 2017. He is currently pursuing the Ph.D. degree with the School of Electrical Engineering, Huazhong University of Science and Technology, Wuhan. His current research interests include control of brushless doubly fed induction generators, parameter identification, and model predictive control of linear induction motors.